Carleton Geology Department

Geology Comps Papers

Carleton College *Year* 2004

An intrusive complex in the Khovsgol-Ulaanbadrakhin Terrane, southeast-ern Mongolia

Joseph Graly
Carleton College,

An Intrusive Complex in the Khövsgöl-Ulaanbadrakhin Terrane, southeastern Mongolia

Joseph Graly
Senior Integrative Exercise
Carleton College
3/8/2004

Table of Contents

Abstract

Southeastern Mongolia is part of the series of volcanic arcs, micro-continents, and accretionary terranes that connects the Siberian craton with the North China block. Within the proposed Khövsgöl -Ulaanbadrakhin terrane, in the northern Toto Shan block, hundreds of dikes intrude a granodiorite pluton. At least six generations of cross-cutting dikes are found in the study area, each with unique magmatic source and structural conditions. Between the first and last dike event, the orientation of least horizontal compressional stress rotated 335° from N20°W to N5°E, with the most voluminous event orientated at N85°W.

Keywords: Dikes, Mongolia, Structural Analysis, Orientation, Petrology, Geochemistry, Magmatic Differentiation

Introduction

Dikes are an historical record of magmatic events. Dike swarms of extraordinary size often correspond to historical mantle plumes, being the feeder conduits for flood basalts and other volcanism (Campbell, 2001). Extensional tectonic stresses and source location determine dike orientation (Campbell, 2001). The dikes of the Khövsgöl-Ulaanbadrakhin Terrane exhibit a complex history of such magmatic events and extensional stress.

Between latitudes 43° 40’ and 43° 50’ and longitudes 109° 45’ and 110° 15’ over 300 dikes intrude a granodiorite pluton. The pluton is surrounded by Upper Cretaceous sedimentary basins (Graham et al., 2001). Dikes vary in composition from quartz-rich granitoids to hornblende leuco-gabbroids and exhibit diverse orientations. The dikes are proposed to be Permian in age and the pluton Carboniferous (Baynaa, 2003).

This study was made possible by a joint 2003 summer expedition between the Keck Geology Consortium and the Mongolian University of Science and Technology. The object of study was the Tavan Khar area, located between latitudes 109° 15’ and 110° 15’ and longitudes 43° 40’ and 44° 10’ (Figure 1). I worked in the field with Molor Erdenebat, a student at the Mongolian University of Science and Technology. We surveyed our study area by Jeep, supplementing our field observations with aerial photographs provided by Cari Johnson (Stanford Universty), and Landsat TM images provided by the University of Maryland Global Land Cover Facility (2003). To my knowledge, no work has been published on this complex.

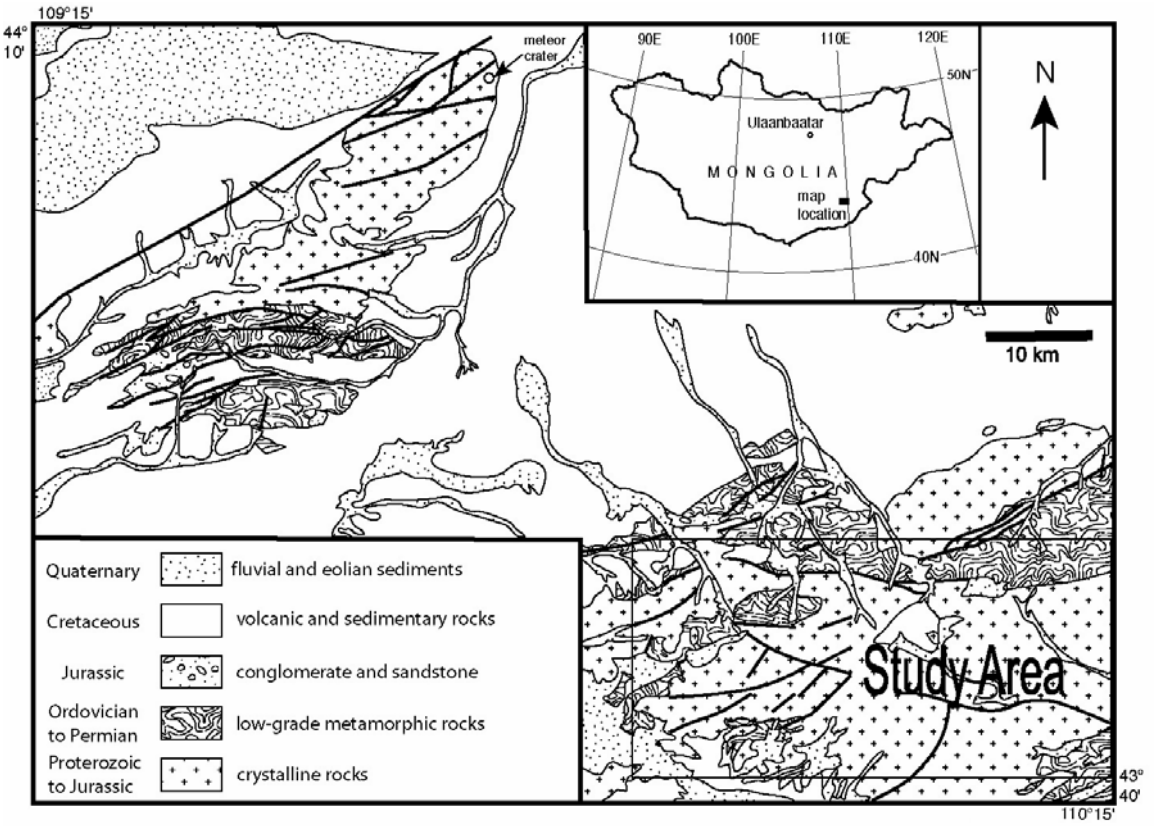

Figure 1. Location and geology of the Tavan Khar Area (modified from Robert Carson's figure in the 2004 Keck publication), Dike clusters are in the southeastern portion labeled Study Area.

Tectonic Setting

Between the stable Precambrian cratons of Siberia, China (both the North and South China blocks), Baltica (the East European Platform), the Arabian platform, and the Indian subcontinent, Central Asia consists of hundreds of accretionary and micro-continent terranes, generally assembled during the middle and late Paleozoic (Heubeck, 2001). The terranes of eastern Mongolia trend approximately East-West and connect the Siberian and North China cratons (Sengör and Natal'in, 1996). Following the Mongolian classification system, the study area is within the Khövsgöl-Ulaanbadrakhin terrane (Bayasgalan, 2003). This terrane, named after the towns of Khövsgöl and Ulaanbadrakh

located therein, is the northern most terrane southeast of the Zuunbayan fault and is part of the Toto Shan uplift block between the East Gobi and Erlian Mesozoic rift basins (Johnson et al., 2001).

Through their study of the composition of Paleozoic clastic sedimentary rocks of southern Mongolia, Lamb and Badarch (2001) propose a series of volcanic arc complexes stretching from the Gobi-Altai to the Toto Shan, active in the Devonian, Carboniferous and Permian periods. The Devonian arc complex is thought to have followed the trace of Mongolia's modern political boundary with China, while by the Carboniferous the western part of the arc complex is thought to have moved south and formed the northern Tian Shan. The eastern complexes stayed within the modern South-gobi province of Mongolia (Lamb and Badarch, 2001). Permian sedimentary records show that volcanic arc rocks are the primary source for sandstones; however, this could be accounted for by the uplift and exposure of Devonian and Carboniferous age volcanic rocks (Lamb and Badarch, 2001). Until the Permian, the Gobi terranes appear to have been located between two subduction zones and their associated arc complexes, one being the southern margin of the Mongolia-Okhotsk (Khangai-Khantey) Ocean and the other being the northern margin of the Solonker Ocean, which was bounded on its southern margin by the North China block (Sengör and Natal'in, 1996).

The late Permian breakup of Pangea initiated extensional regimes world wide. However, modern Mongolia appears to have experienced shortening during this period. The Mongolia-Okhotsk basin closed and the North China block collided with the Siberian continent in late Permian time (Zorin et al., 1993). Thus, the Devonian and Carboniferous arcs were accreted onto the Siberian continent, and became locked within

the continental interior. As evidenced by synorogenic fluvial and lacustrine deposits, collisional uplift and shortening continued through the Triassic and possibly until the lowermost Jurassic (Hendrix et al., 2001). Left lateral displacement along the Zuunbayan and other regional faults dominated through the middle Jurassic, accommodating at least 185 kilometers of displacement (Lamb et al., 1999). Sedimentary sequences in Khar Khotol and other locations show that extension occurred during the Early Cretaceous (Johnson et al., 2001). No significant later tectonic activity is documented in the east Gobi region of Mongolia. However, evidence for a quaternary fault was discovered during the 2003 Keck expedition (Kast and Manchuk, 2004).

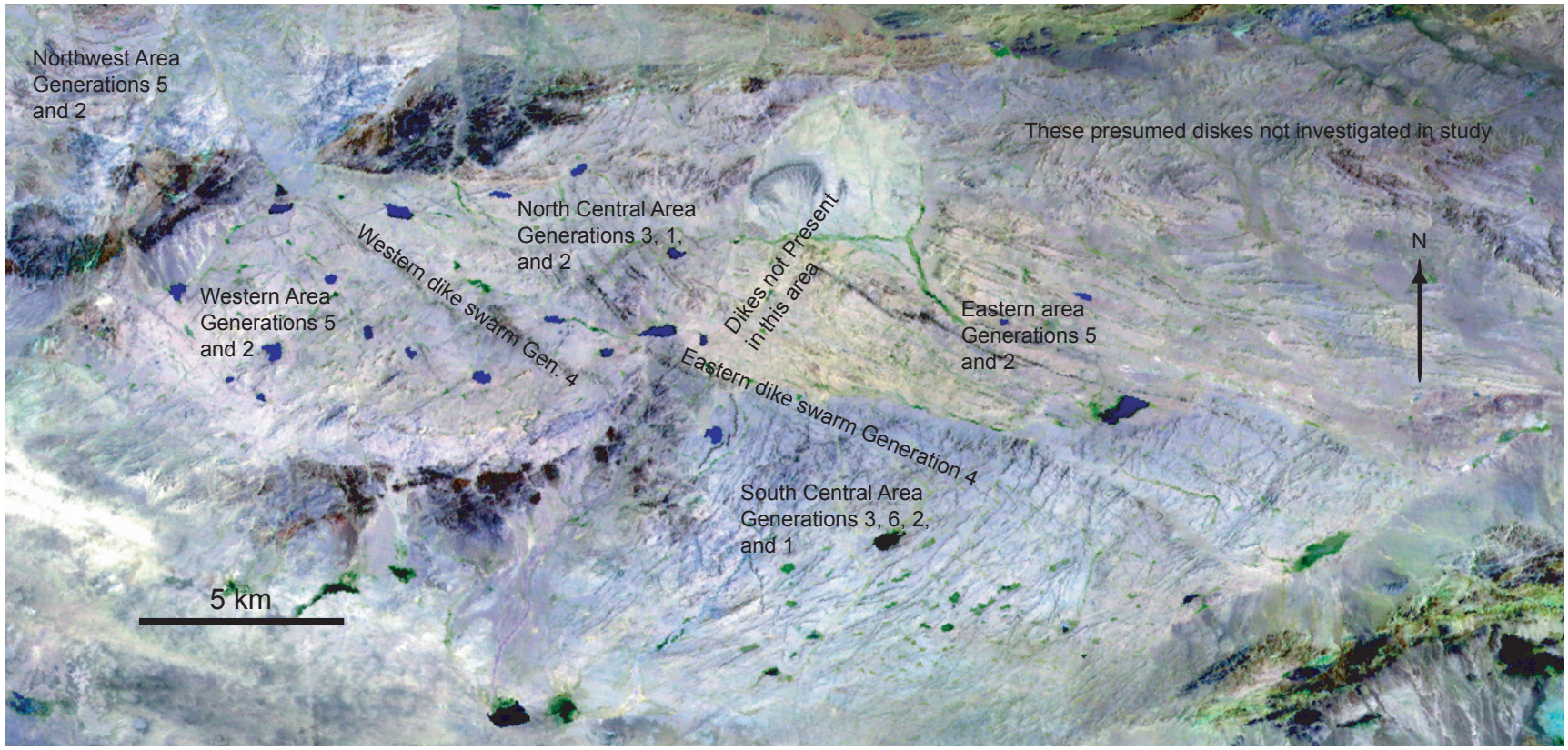

Figure 2. Landsat TM (7,5,3) image showing regional distinctions within the field area.

Field Relationships and Petrography of the Khövsgöl – Ulaanbadrakhin Dikes

At least six generations of dikes are found within the study area. "Generation" as used here implies a cluster of dikes of similar composition, size, and orientation. Dikes within a generation typically do not cross-cut each other and hold consistent cross-cutting relationships to dikes of other generations. Dikes within a generation are typically parallel, meaning that dikes intrude at identical or near-identical orientations and are approximately equidistant from one another. Crosscutting dike generations are assumed to be younger than the dike generations they cut.

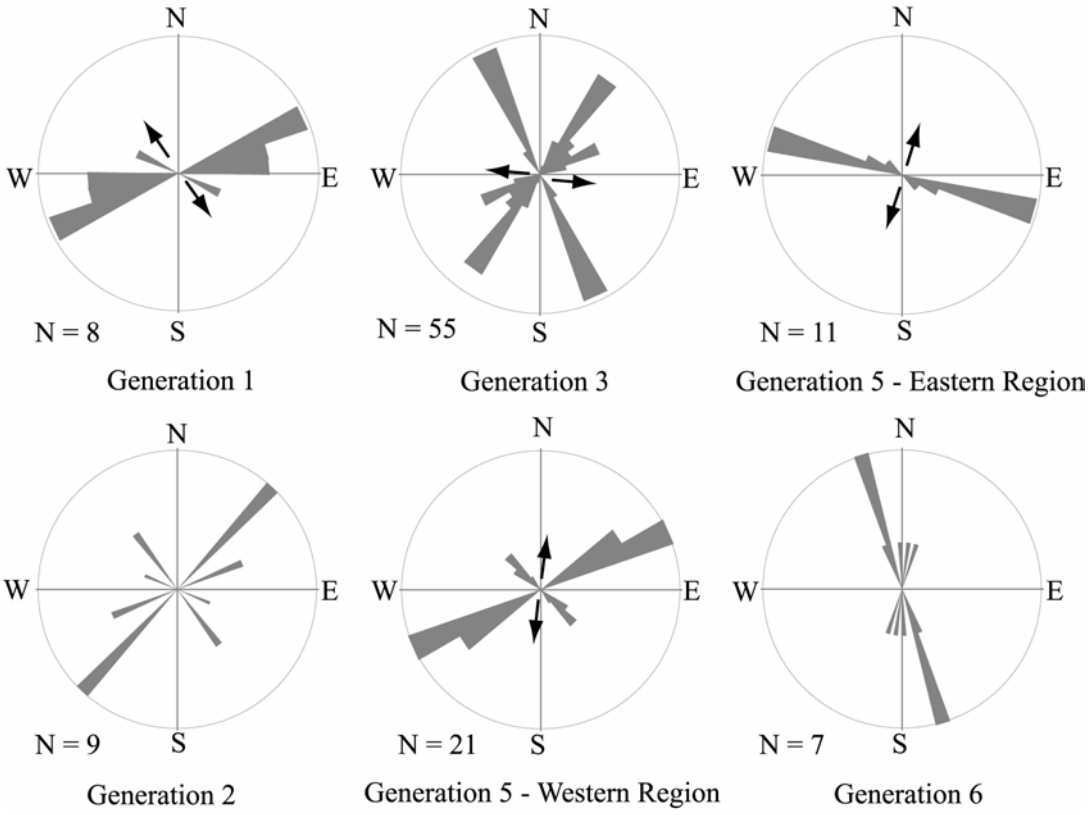

Figure 3. Rose diagram of dike orientations measured in the field, observed through aerial photography, or observed through TM imagery. Arrows indicate approximate direction of least principle horizontal compressive stress (see discussion).

The oldest dikes are coarse-grained felsic rocks, varying from quartz-rich granitoids to granodiorites, and are generally between 1 and 10 m thick. Dikes of this generation are found in the north central and south central areas (Figure 2). First generation dikes are cut by either second or third generation dikes. The coarse grained felsic nature of the first generation dikes makes them nearly as subject to erosion as the pluton and therefore difficult to detect through aerial photography. Dikes confirmed to be of this generation generally strike between N70°E and N90°E (Figure 3).

The second generation of dikes is mafic, fine-grained hornblende leuco-gabbros between 1 and 10 m thick. Throughout the western and central areas, dikes generally strike N40°E. However, in the northern and eastern regions, probable second generation dikes strike in diverse orientations (Figure 3). Some dikes of this generation are sinuous. These dikes, being thin, do not appear on available TM imagery. Their orientation therefore has not been well studied in the eastern portions of the study area, where aerial photography is unavailable. The second generation is observed to be cut by fifth generation dikes in the eastern and western areas, third generation dikes in the central areas, sixth generation dikes in the south central area, and by the fourth generation eastern and western dike swarms (Figure 2).

Third generation dikes are between 10 and 100 m thick and are mafic or intermediate in composition. Most of these dikes are amphibole-bearing diorites, though at least two dikes are substantially more felsic. Third generation dikes dominate the north central and south central areas (Figure 2). The north central dikes strike around N30°W, while the south central dikes typically strike between N40°E and N70°E (Figure 3). The two groups are assumed to be co-generational based on similarity in size and

composition. Third generation dikes are cross-cut by sixth generation dikes and by the fourth generation eastern dike swarm. While most third generation dikes intrude parallel to each other, there are places were parallel dikes bend inward, cross cut each other, and then continue onward in parallel forming a bowtie-like formation (Figure 4).

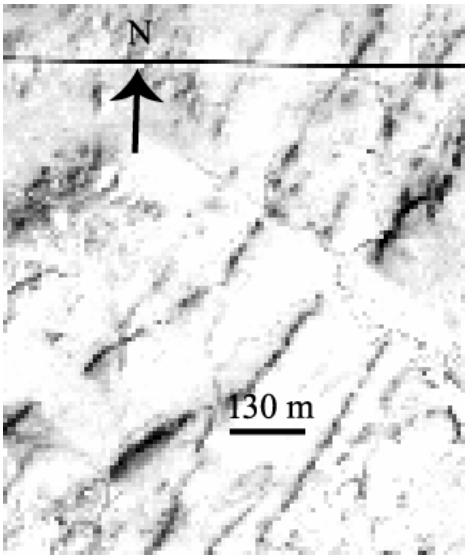

. Figure 4. Aerial photograph showing bowtie formations in third generation dikes.

The fourth generation consists of two dike swarms that bisect the study area (Figure 2). The western swarm is approximately 10 km long, strikes N32°W in an en echelon fashion, and consists of at least 14 parallel dikes. The eastern swarm is about 7 km long, contains at least 19 parallel dikes and strikes N57°W. Dike composition varies within the swarms. The western swarm is more felsic, with compositions ranging from granodiorite to diorite. The compositions of the eastern swarm range from quartz-diorite to gabbro. I categorized the swarms as a single generation, because both are observed to be cut by fifth generation dikes. This is not meant to necessarily suggest that two swarms are otherwise related. As the two swarms do not intersect each other, relative age cannot be determined from field relationships.

The fifth generation consists of granitoid dikes typically between 10 and 100 m thick. Most of these dikes are significantly finer grained than the felsic dikes of the first generation. These dikes predominate in the western and eastern areas (Figure 2). In the western area, dikes either strike approximately N50°W or approximately N60°E (Figure 3). In the eastern area, dikes strike approximately N75°W (Figure 3). Presumed fifth generation dikes are also found in the northwest area, where they cut possibly second generation mafic dikes. The dikes in the northwest area form an arcuate pattern that arcs southward from N60°E to N40°W. The dikes are posited as co-generational due to similarities in size and composition. The eastern dikes do not intersect generations three or four. The western dikes do not intersect generation six, while possible eastern dikes do. Thus, respective age relationships to respective generations are not known. The lack of matching structural orientation between the three regions of later felsic dikes suggests that they perhaps represent disparate events and therefore may not be related in age.

The sixth generation consists of 10 -100 m thick diorite dikes. These dikes occur only in the south-central portion of the study area (Figure 2). Dikes radiate from strikes of N20°W in their western most occurrence to N8°E in their eastern most occurrence (Figure 3). This is the only generation that has a fanning geometry.

In every generation of dikes, some dikes intrude in an en echelon fashion. The displacement and frequency of these en echelon structures are greatest in the western dike swarm and in the southern portion of the south central area (Figure 2). Anderson (1963) proposes that en echelon structures indicate different stress orientations at the base and surfaces of dikes (Figure 5). The western dikes swarm has a base orientation of N54°W, which differs notably from the average orientation of the various individual echelons that

generally strike N42°W. The base orientation for many sixth generation dikes is five to two degrees further west than the surface orientation. Third generation dikes of the southern portion of the south central area typically have base orientations five to ten degrees more northerly than their surface orientations. Many of these surface orientations strike around N70°E and if plotted as base orientations would strike N60°E. In the south central area large third and sixth generation dikes exhibit a curved structure, either of base or surface orientations (Figure 6).

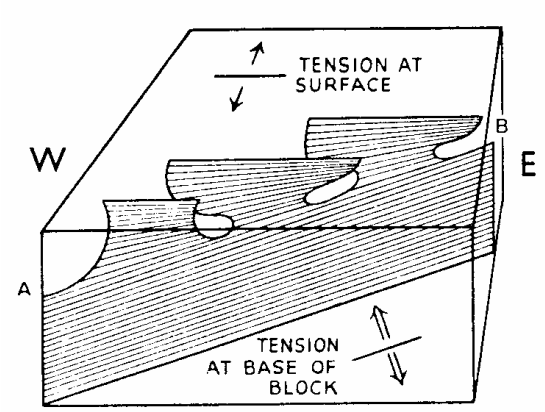

Figure 5. Anderson's (1963) schematic for tensional control of the structure of en echelon dikes.

In multiple locations the dikes incorporate material of differing lithologies. In one case mafic material is incorporated into a felsic dike. In two cases felsic material is incorporated into a mafic dike. In both felsic cases the material was confirmed to have a lithology differing from the pluton. These appear to be xenoliths, as there is no evidence of magma mixing.

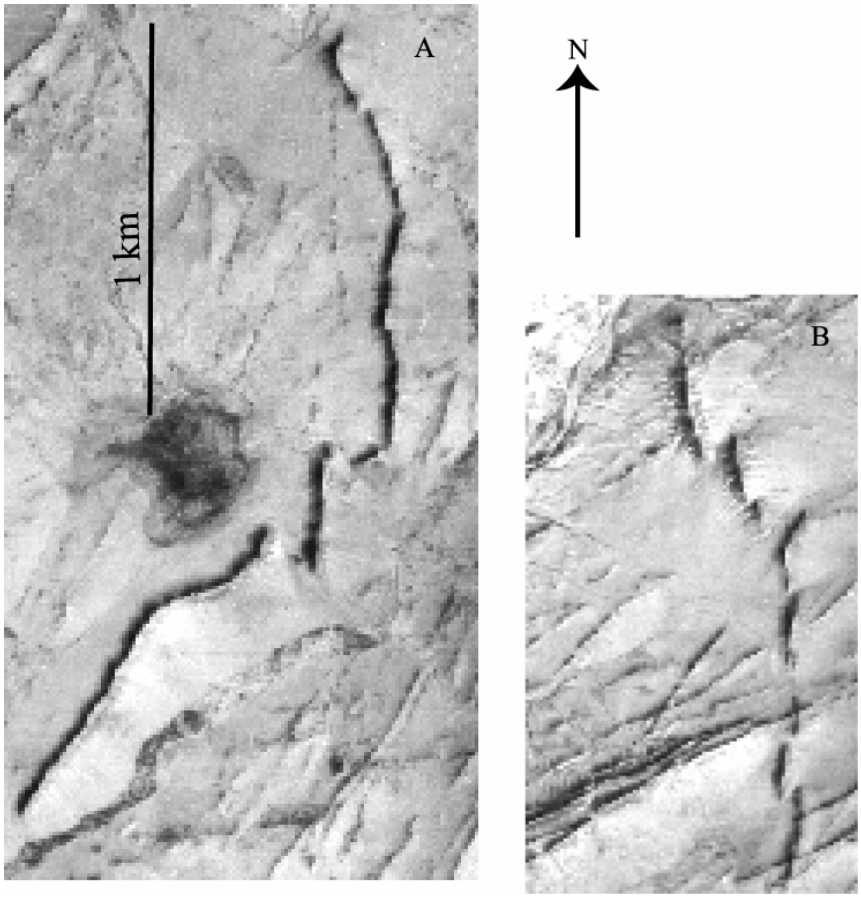

Figure 6. Aerial photographs showing arcuate geometries in the south central area. (a): Third generation dike 1. (b) Sixth generation dike 3A.

Landsat TM imagery reveals apparent dike clusters elsewhere in the Toto Shan block (Figure 7a). Some of these dikes do not occur in granite bodies but in volcanics presumed to be Devonian (Lamb et al., 1999). These are located in the central (Figure 7b) and southwestern (Figure 7c) Toto Shan. Granitic outcrops north of the study area, separated from the studied granodiorites by Carboniferous sedimentary rocks (Baynaa, 2003), also contain apparent dikes (Figure 7d). Similar granitic rocks outcrop some 200 km southwest of the study area, offset by Jurassic strike-slip faulting (Lamb and Badarch, 2001). Landsat TM imagery reveals that this region also contains apparent dikes with complex orientation and cross-cutting relationships (Figure 7e).

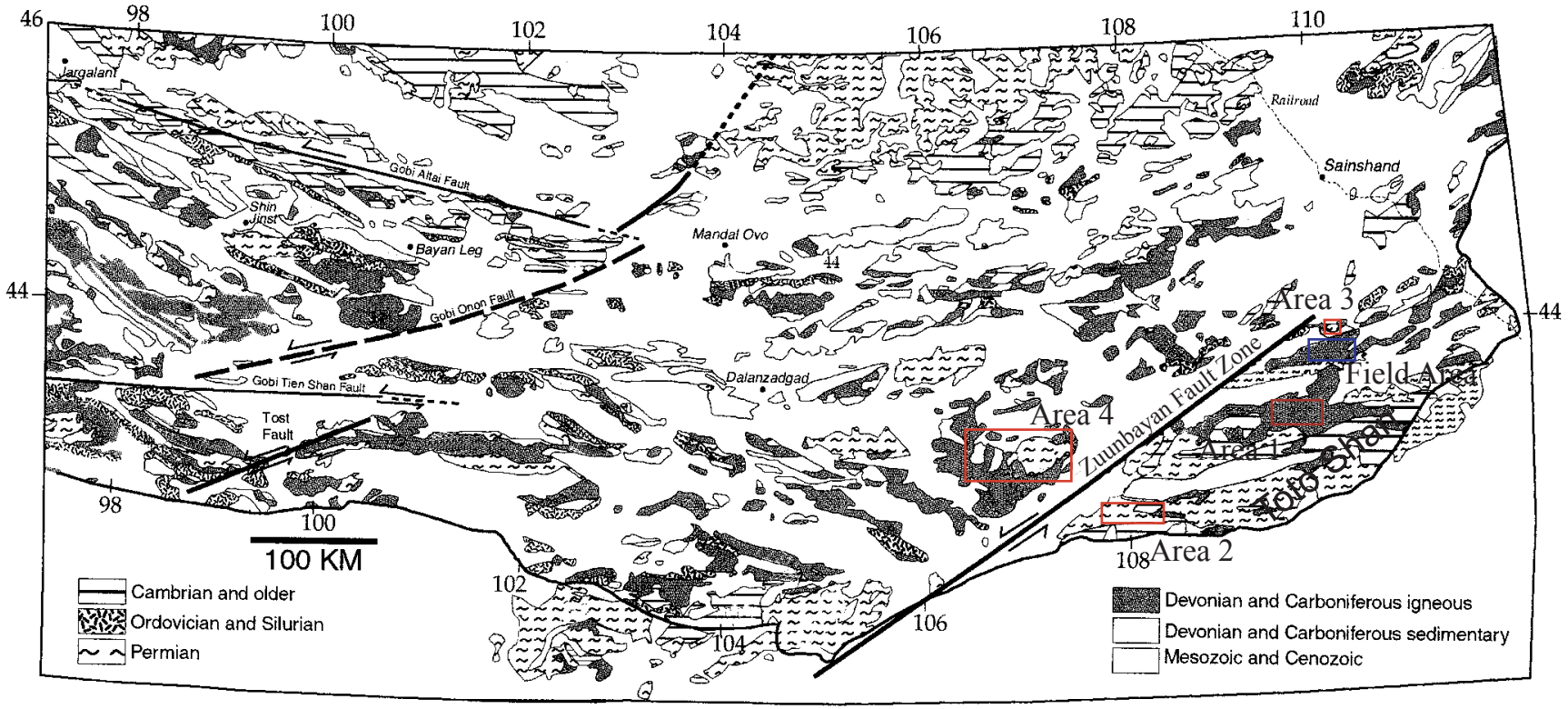

Figure 7. Locations of apparent dikes revealed through landsat TM images. (a) Geologic Map of southern Mongolia modified from Lamb et al. (1999) showing locations of areas containing apparent dikes in and near the Toto Shan. (b) Area 1: Landsat TM (7,5,3) image showing apparent dikes in Devonian volcanics of the central Toto Shan. (c) Area 2: Landsat TM (7,5,3) image showing apparent dikes in the southwest Toto Shan, near China. (d) Landsat TM (7,5,3) image showing apparent dikes north of the field area separated by Carboniferous sediments. (e) Area 4: Landsat TM (3,2,1) image showing apparent dikes southeast of field area displaced by the Zuunbayan Fault.

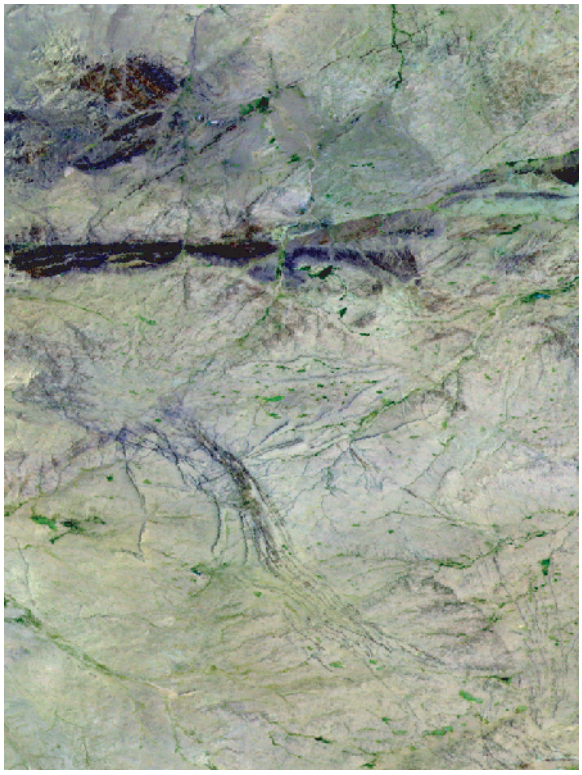

B: Area 1

D: Area 3

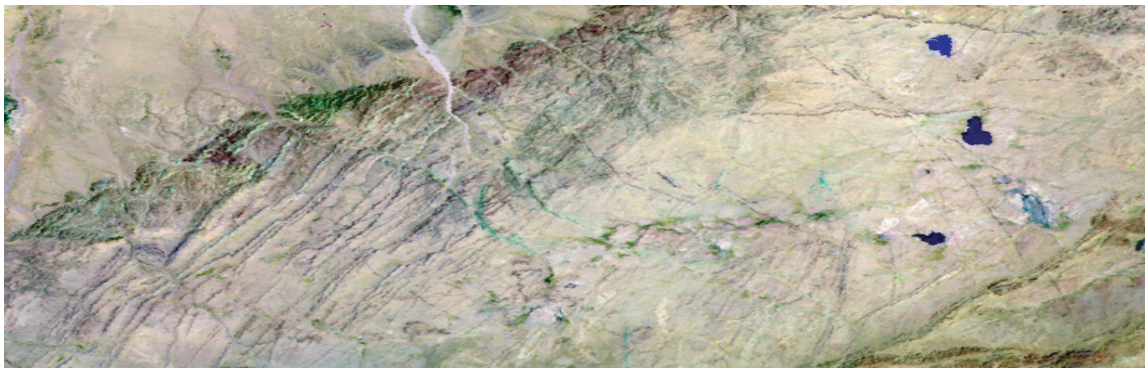

C: Area 2

E: Area 4

Figure 7 - continued.

Table 1: Alteration patterns in dikes with greater than ten percent alteration of ferromagnisum minerals.

Sample	Location	Gen.	% Alt.	Epidote	Chlorite	Prehnite	Dolomite	Notes
3A	South-Central	6	100	Lots	Lots	Lil	None	
5G	South-Central	3	98	Lots	Lots	Lil	None	Unusally felsic for gen 3
5B	South-Central	2	80	Some	Some	Lil	Some	
6B	South-Central	3	70	Lots	Some	None	None	
6G	South-Central	?	98	Some	Lots	None	None	
7	South-Central	3	>100	Lots	Some	?	None	Probable Metasomatism
10	Eastern	5	See note	None	None	Lots	None	Appox. No Fe Content
10B	Eastern	2	100	Some	Lots	Lil	Some	
11C	South-Central	1	100	Lil	None	Lots	None	Very little Fe Content
15A	South-Central	1?	100	Some	Some	Some	None	
15B	South-Central	?	100	Lots	Lots	None	None	
17	South-Central	1?	35	Some	Some	Some	None	Very little Fe Content
25B	Western Dike Swarm	4	100	Lots	Lots	Some	None	
25C	Western Dike Swarm	4	90	Lots	Some	Lots	None	
27A	Western	2	15	Some	Lil	?	None	
27B	Western	5	>100	Lots	Lots	None	None	Probable Metasomatism
29	Northern	1	100	Some	Lots	Some	None	Possible Metasomatism
30	North-Central	1	90	Some	Some	Lil	None	Very little Fe Content
31	North-Central	3	100	Lots	Lots	?	None	Possible Metasomatism
33	Eastern Dike Swarm	4	70	Lots	Lots	Some	Some	
33M	Eastern Dike Swarm	4	50	Lil	Lots	Some	Some	
33I	Eastern Dike Swarm	4	95	Some	Lots	Lots	Some	
34A	Southeastern	4	95	Some	Lots	Some	Some	
34B	Southeastern	3	See note	Lil	None	Lots	None	Appox. No Fe Content
34C	Southeastern	2	95	Some	Lots	Lil	Lots	

Lots: >20% Some: 1-20% Lil: <1%

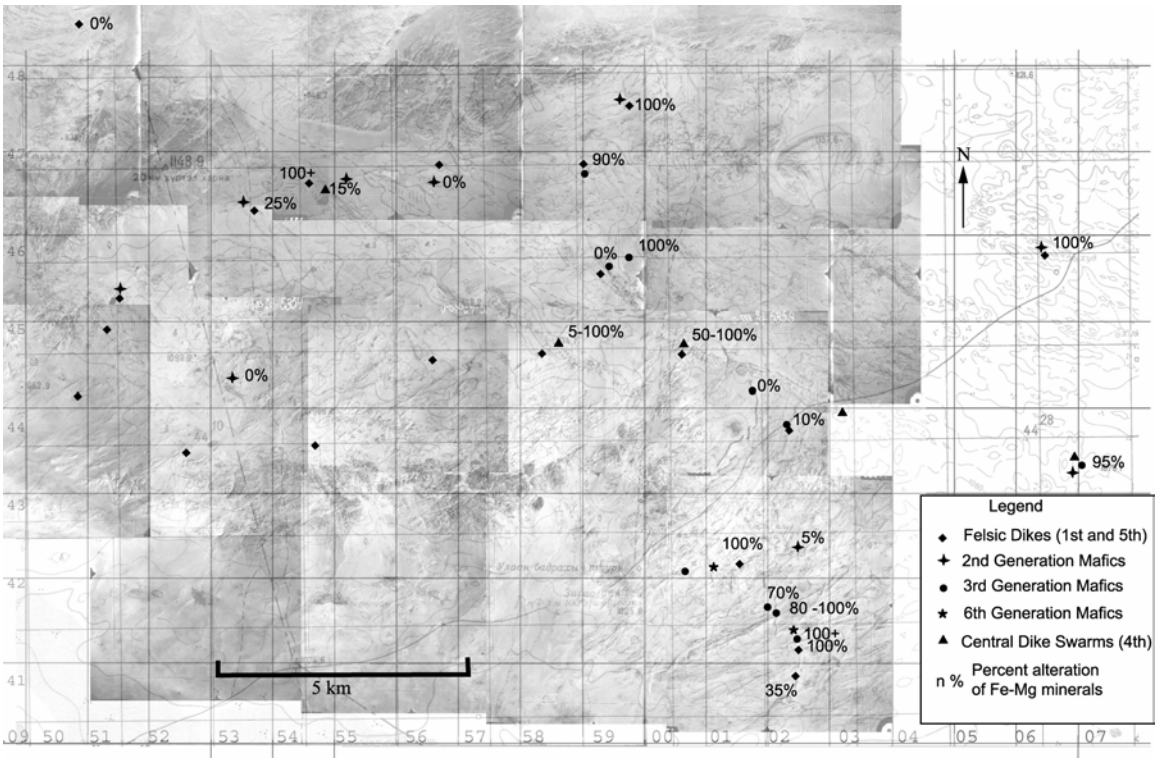

Figure 8. Topographic map overlain by aerial photograph showing location and generation of field confirmed dikes and percent alteration of ferromagnesium minerals.

Many studied dikes contain prehnite, epidote, chlorite, dolomite, or combinations of the four (Table 1). Quantities of epidote and chlorite are restricted by quantities of Fe and Mg in the protolith. Therefore, an estimation of the absolute percentage of alteration minerals would more represent original percentages of ferromagnesium minerals than alteration. Displayed percentages (Figure 8) represent ratios of quantities unaltered ferromagnesium minerals (most often amphiboles) to quantities of chlorite, epidote, and dolomite. 100+ indicates that the quantities of epidote in the sample seem to exceed the amount ferro-magnesium available in protolith minerals.

Geochemistry

Twelve samples from diverse generations and field locations (Table 2) were analyzed with X-ray florescence and inductively coupled plasma mass spectrometry for major (Table 3), trace (Table 4), and rare earth element (Table 5) content.

Table 2: Location and generation of samples subject to geochemical analysis.

Sample	Generation		Location	
1	3		Central	
3A	6		South Central	
5	3		South Central	
7	3		South Central	
10	5		Eastern	
17	1	?	South Central	
25B	4		Western Dike Swarm	
28C	2		Northern	
30	1		North Central	
32	3		North Central	
33	4		Eastern Dike Swarm	
33M	4		Eastern Dike Swarm	

Table 3: Major Element percentages

Sample	SiO2	TiO2	Al2O3	Fe2O3	MnO	MgO	CaO	Na2O
1	60.00	1.16	15.78	6.57	0.10	2.09	5.73	4.66
3A	66.24	0.34	15.62	3.31	0.06	1.60	4.10	3.78
5	70.39	0.27	15.60	2.29	0.04	1.21	2.49	5.42
7	54.56	1.21	17.41	8.16	0.13	3.84	7.41	4.26
10	74.81	0.05	13.05	1.10	0.07	0.10	0.32	3.98
17	75.77	0.09	12.89	2.34	0.03	0.13	0.54	4.06
25B	70.97	0.30	14.88	3.03	0.06	0.80	2.08	4.23
28C	67.63	0.56	15.89	3.79	0.09	0.96	2.77	5.19
30	77.64	0.06	12.27	0.76	0.01	0.09	0.68	2.90
32	60.05	0.64	18.74	5.90	0.09	2.97	6.65	4.07
33	61.00	0.65	16.73	5.49	0.10	2.43	5.31	3.90
33M	60.84	0.63	16.38	5.51	0.11	2.87	5.01	3.94

Table 4 – Continued:

Sample	K2O	P2O5	LOI	Total
1	1.67	0.43	1.86	100.05
3A	2.14	0.12	1.19	98.50
5	1.51	0.09	1.36	100.67
7	0.78	0.32	1.66	99.74
10	3.34	0.02	0.55	97.39
17	4.65	0.03	0.00	100.53
25B	3.28	0.11	0.56	100.30
28C	2.50	0.20	0.45	100.03
30	5.58	0.02	0.00	100.01
32	0.44	0.15	0.98	100.68
33	1.42	0.16	2.21	99.40
33M	1.92	0.21	2.27	99.69

Table 4: Trace element data parts per million Negative numbers are below lower limit

Sample	V	Cr	Co	Ni	Cu	Zn	Ga	Ge	Rb	Sr	Y	Zr	Nb	Sn	Cs	Ba
1	156	-20	13	-20	12	137	20	2	40	467	29	218	14	1	1.2	456
3A	62	35	8	24	11	94	17	2	61	695	14	140	9	-1	1.1	710
5	44	29	6	-20	22	90	18	1	40	448	7	123	5	-1	0.6	232
7	164	79	16	72	27	58	20	1	11	640	27	230	5	1	-0.5	328
10	10	-20	-1	-20	-10	-30	17	2	177	71	13	71	9	3	7.6	249
17	16	21	2	-20	16	-30	16	3	104	47	11	62	8	3	1.7	195
25B	32	-20	5	-20	12	35	14	2	103	254	16	172	6	2	2.0	643
28C	29	-20	3	-20	-10	73	19	2	58	361	23	344	9	2	2.3	644
30	9	-20	-1	-20	-10	-30	11	2	112	174	4	72	3	-1	0.6	977
32	102	39	15	36	18	74	19	1	10	958	10	71	3	-1	-0.5	291
33	104	24	12	25	27	87	18	2	40	496	15	133	4	1	1.4	427
33M	108	48	16	37	26	64	18	1	45	648	17	148	4	1	1.5	526

Table 5 – Continued:

Sample	Hf	Ta	Tl	Pb	Th	U
1	4.7	0.4	0.4	10	4.5	1.5
3A	3.3	0.4	0.5	10	5.1	1.7
5	2.9	-0.1	0.4	8	1.2	0.8
7	4.8	0.2	-0.1	-5	1.7	0.9
10	2.5	1.0	1.4	29	9.4	1.1
17	2.9	0.8	0.6	18	10.0	0.9
25B	4.2	0.7	0.8	12	13.4	4.1
28C	7.1	0.6	0.5	12	6.6	2.4
30	2.5	0.2	0.8	11	18.1	1.6
32	1.8	0.1	-0.1	-5	1.1	0.3
33	3.3	0.3	0.3	6	3.9	1.2
33M	3.4	0.3	0.3	-5	5.4	1.6

Table 5: Rare Earth Element data parts per million.

Sample	La	Ce	Pr	Nd	Sm	Eu	Gd	Tb	Dy	Ho	Er	Tm	Yb	Lu
1	21.7	47.0	5.89	24.4	5.6	1.62	5.2	0.9	4.8	1.0	2.9	0.42	2.7	0.40
3A	17.1	33.7	3.68	13.7	2.7	0.76	2.4	0.4	2.2	0.4	1.3	0.21	1.3	0.21
5	7.5	16.7	2.00	8.3	1.9	0.64	1.8	0.3	1.3	0.2	0.6	0.09	0.6	0.08
7	14.1	30.9	4.40	20.1	5.0	1.91	5.1	0.9	4.8	1.0	2.8	0.42	2.6	0.39
10	4.8	14.8	1.30	4.9	1.5	0.20	1.7	0.3	2.1	0.4	1.5	0.25	1.6	0.26
17	8.2	21.0	1.87	6.9	1.7	0.22	1.6	0.3	1.7	0.3	1.2	0.20	1.4	0.22
25B	20.9	41.2	4.45	16.3	3.3	0.70	2.8	0.5	2.6	0.5	1.7	0.28	1.8	0.30
28C	26.3	55.8	6.14	23.3	4.6	1.35	3.8	0.7	3.7	0.8	2.4	0.39	2.5	0.41
30	9.5	14.0	1.28	4.0	0.7	0.29	0.6	-0.1	0.5	0.1	0.4	0.07	0.5	0.09
32	7.9	16.4	2.03	8.6	1.9	0.77	1.9	0.3	1.7	0.3	1.0	0.14	0.9	0.13
33	16.8	34.7	4.00	15.8	3.4	0.96	3.0	0.5	2.7	0.5	1.6	0.24	1.4	0.23
33M	20.6	41.9	5.07	19.9	4.2	1.17	3.5	0.5	2.9	0.6	1.7	0.25	1.6	0.25

Due to the pervasive alteration that may have mobilized elements like sodium and potassium (Rollinson, 1993), major elements are plotted on Winchester and Floyd's (1977) variation diagram for immobile elements (Figure 9).

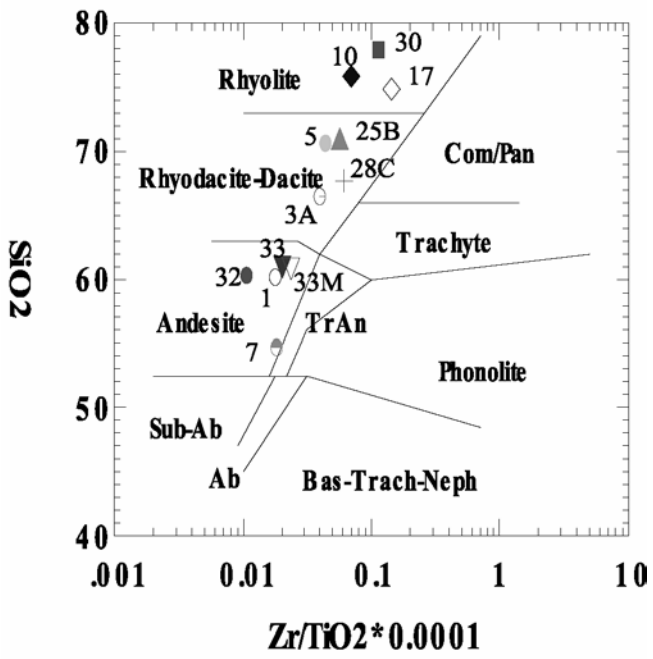

Figure 9. Rock classification of samples on the basis of Winchester and Floyd's (1977) diagram.

Zirconium and Hafnium have similar partition co-efficients, as do Niobium and Tantalum (Rollinson, 1993). Therefore, the ratios of the pairs are plotted against each

other. Samples with similar melt fractionation conditions should plot similarly. The data appears to form three clusters (Figure 10).

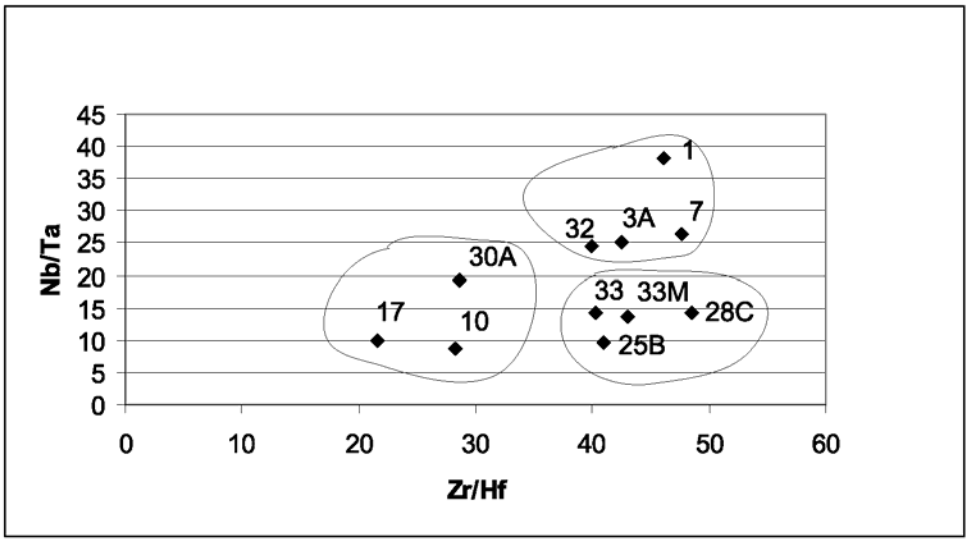

Figure 10. Zirconium/hafnium vs. niobium/tantalum. Samples in circled areas might be genetically related.

Rare earth element data normalized to chondrite values following Boynton (1984) are plotted by the clusters isolated through the previous method (Figures 11-13). Sample 25B shows a markedly different distribution from the other samples of its cluster, chiefly characterized by a Europium deficiency (Figure 11). Samples 10 and 17 are also characterized by Europium deficiencies (Figure 13). However when the rare earth element data are normalized to the values of sample 25B, samples 10 and 17 differ markedly from 25B, having larger Europium deficiencies and notably different distributions of the first five elements (Figure 14). Samples 32 and 7 differ from their cluster (Figure 12), having smoother descents and Europium enrichment. When cluster members are normalized to the values of sample 32 (Figure 15), sample 7 shows a matching trend, with sample 1 being a debatable case. Sample 30 shows a trend that does not at all resemble the trends of samples 10 and 7 (Figure 13). Samples 33, 33m, and

28C from the lower right cluster have reasonable matches with samples 1, 5, and 3a from the upper cluster as demonstrated by normalizing values to sample 3A (Figure 16).

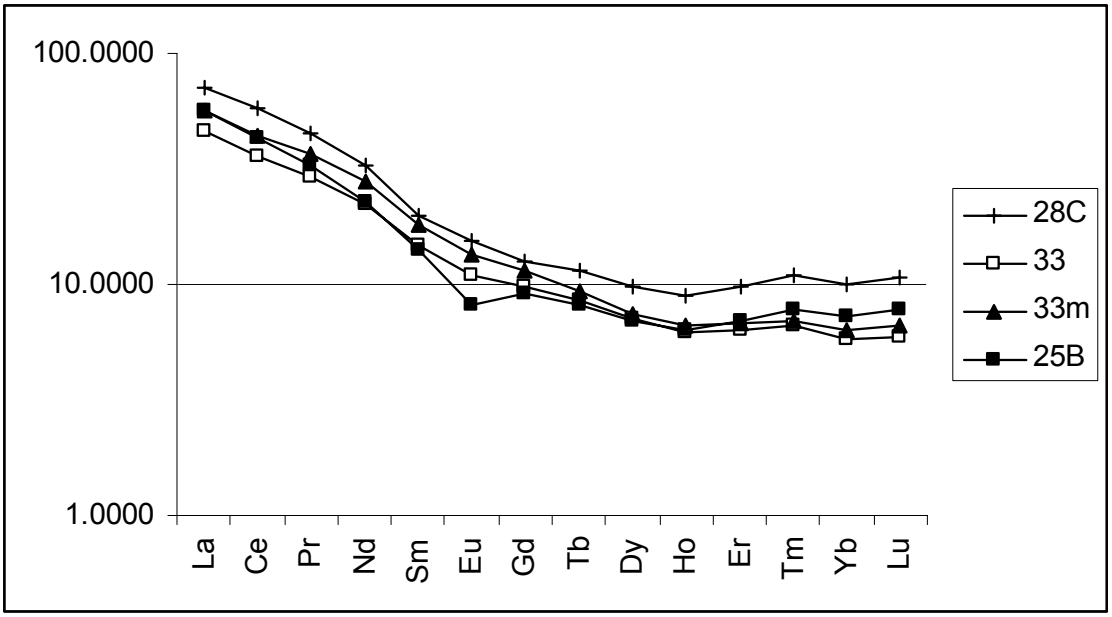

Figure 11. REE data for lower right cluster.

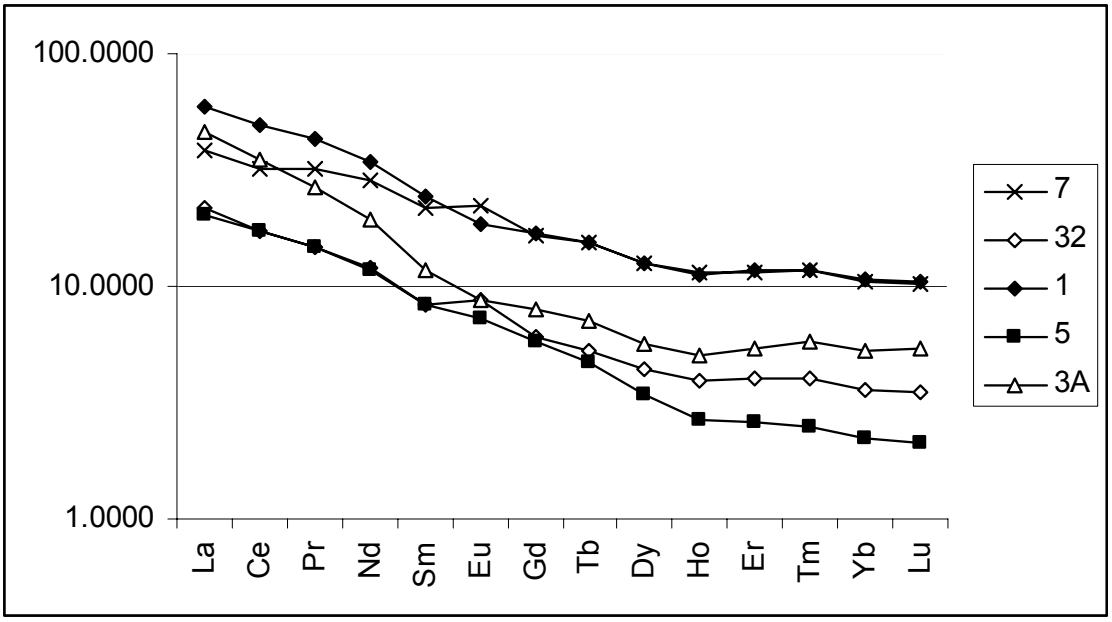

Figure 12. REE data for upper cluster.

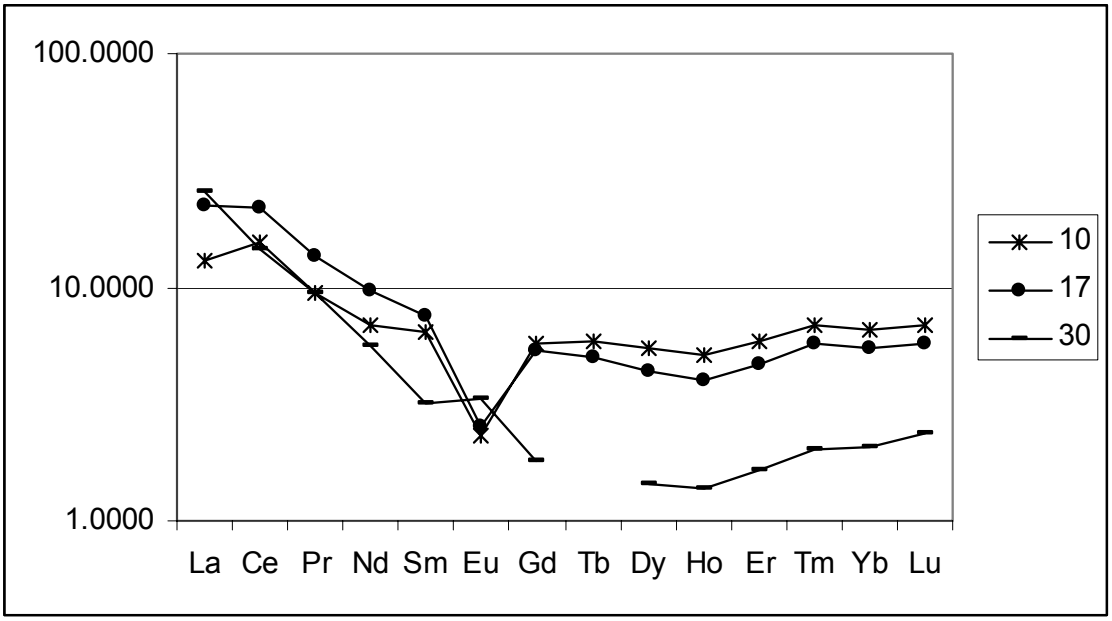

Figure 13. REE data for lower left cluster.

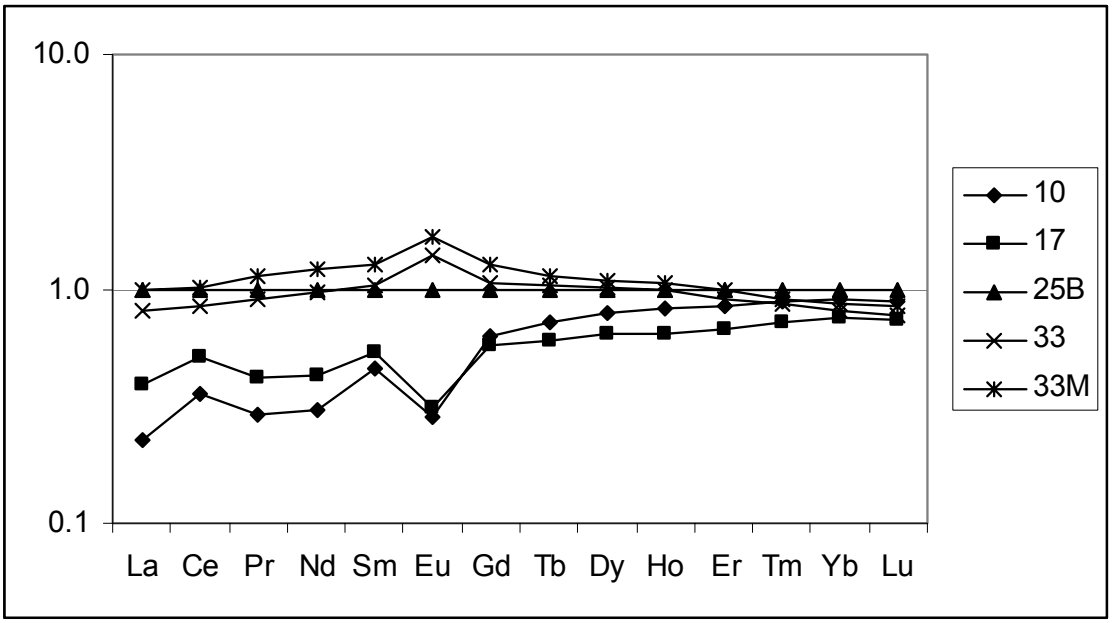

Figure 14. 5th and 4th generation normalized to 25B.

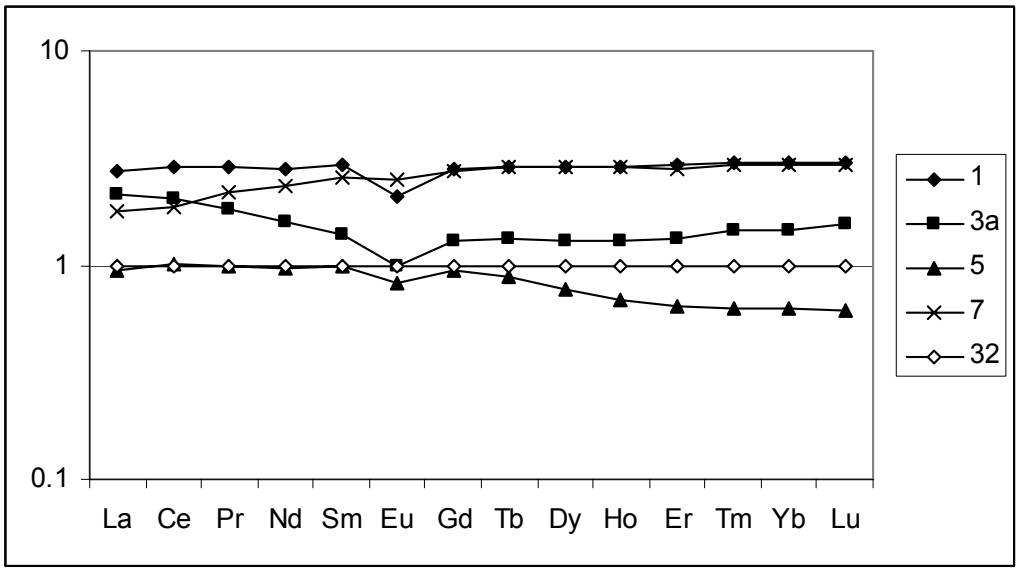

Figure 15. Upper cluster normalized to 32.

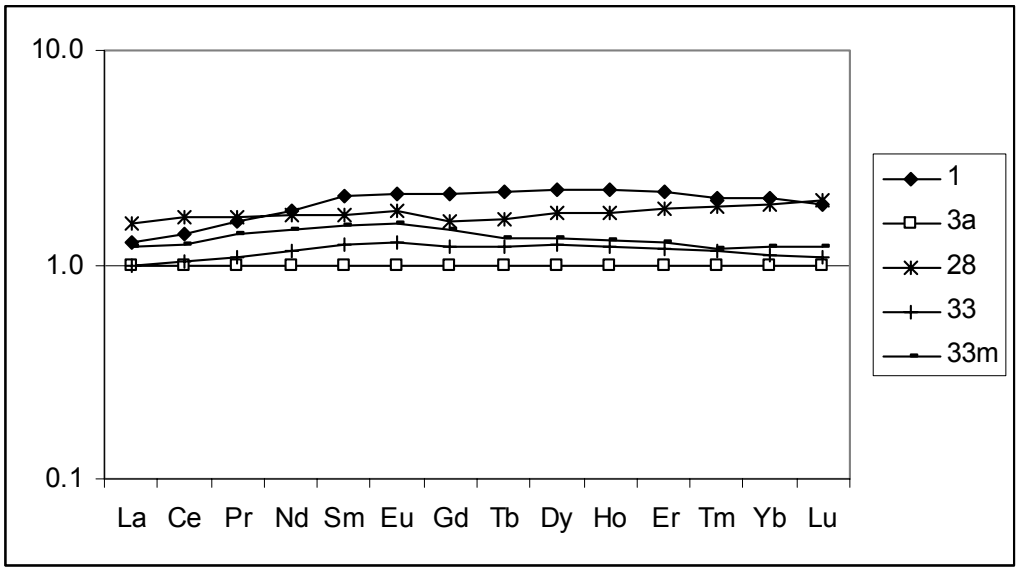

Figure 16. Related dikes normalized to 3A.

Selected trace element data normalized to averaged values for mid ocean ridge basalts (following Rollinson, 1993) and compared to averaged values for upper crustal rocks, lower crustal rocks, and plume enriched mid ocean ridge basalts in Figure 17. Samples 7 and 32 are enriched in Barium as typical of lower crustal rocks (Taylor and McLennan, 1981). All other samples have distribution more closely resembling upper crustal material (Weaver and Tarney, 1984).

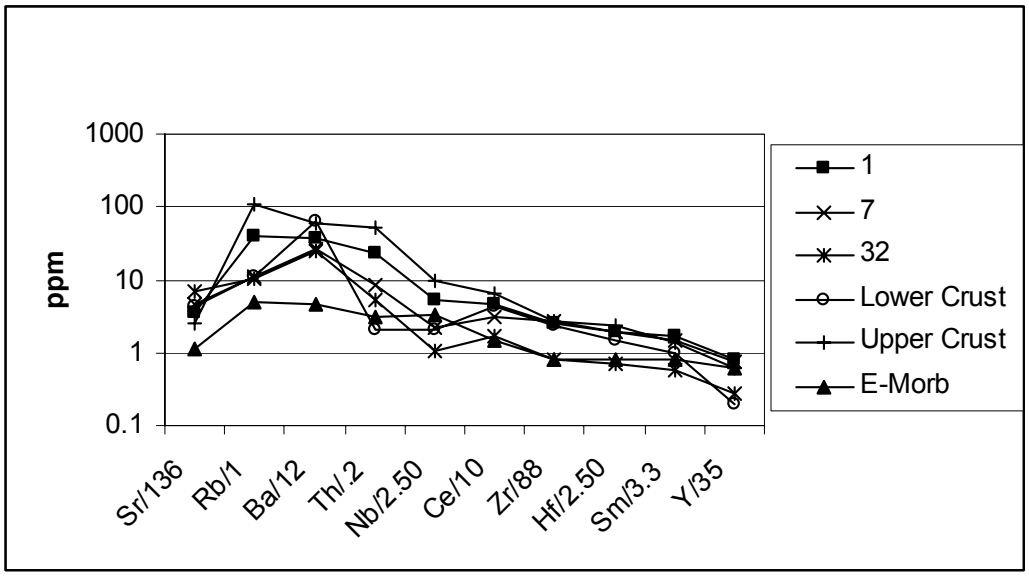

Figure 17: 3rd generation MORB norm (Sun and McDonough, 1989) and averaged values for enriched MORB (Sun and McDonough, 1989), lower crustal rocks (Taylor and McLennan, 1981), and upper crustal rocks (Weaver and Tarney, 1984).

The heterogeneity of the samples and small number of geochemical analyses does not make them ideal for tectonic discrimination, as such diagrams are best suited for results generated from a large suite of relatively homogonous samples (Rollinson, 1993). However, since no work has been done on the tectonic setting of the Khövsgöl-Ulaanbadrakhin dikes, I will present appropriate analyses under the caveat that more geochemical work would produce more reliable tectonic discrimination.

Using available published mechanisms for the analysis of granitoid rocks, samples generally plot within fields that indicate a volcanic arc setting. As trace element analysis was only performed on three granitic samples, the results are limited. Four plots proposed by Pearce et al. (1984) compare quantities of Y, Nb, Yb, Ta, and Rb (Figure 18). Two plots proposed by Harris et al. (1986) compare quantities of Rb, Hf, and Ta (Figure 19). Sample 10 plots as a syn-collisional granite on Harris' diagram.

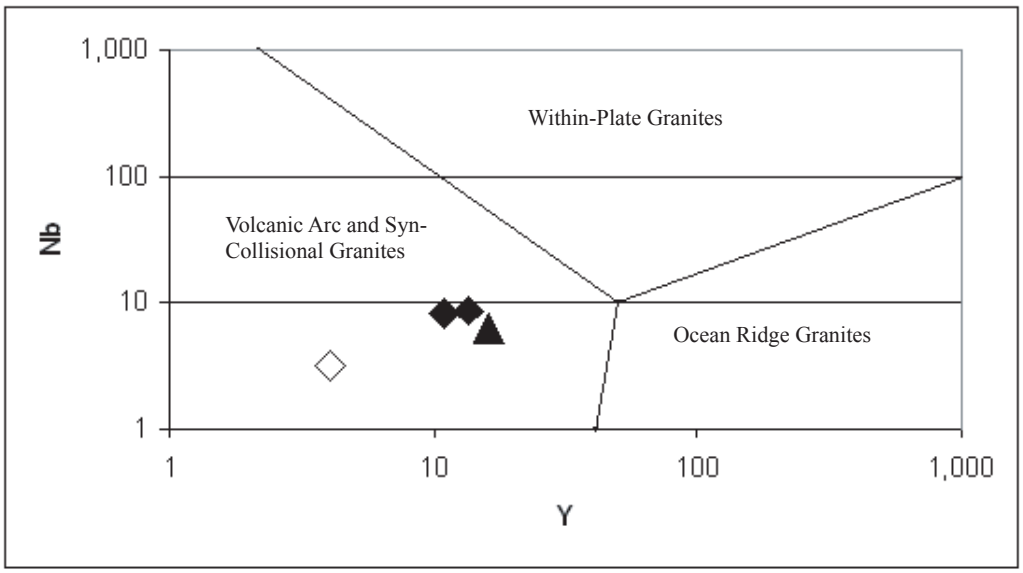

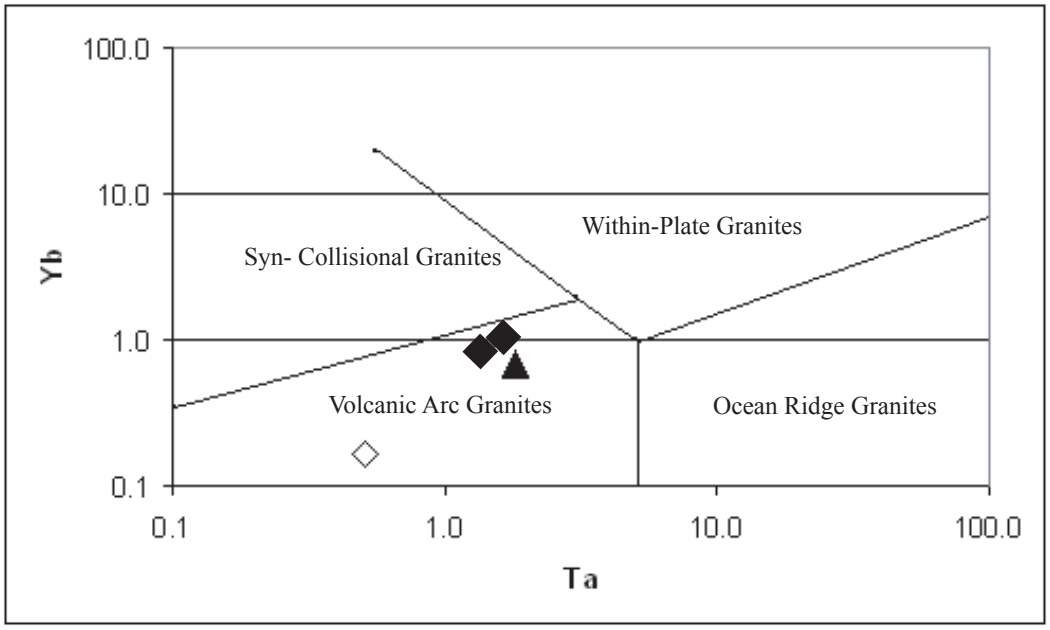

◆ Fifth Generation Granites ▲ Fourth Generation Felsics

◇ First Generation Granites

Figure 18. Felsics plotted on Pearce et al.'s (1984) tectonic discrimination diagrams for granitic rocks. All units are parts per million.

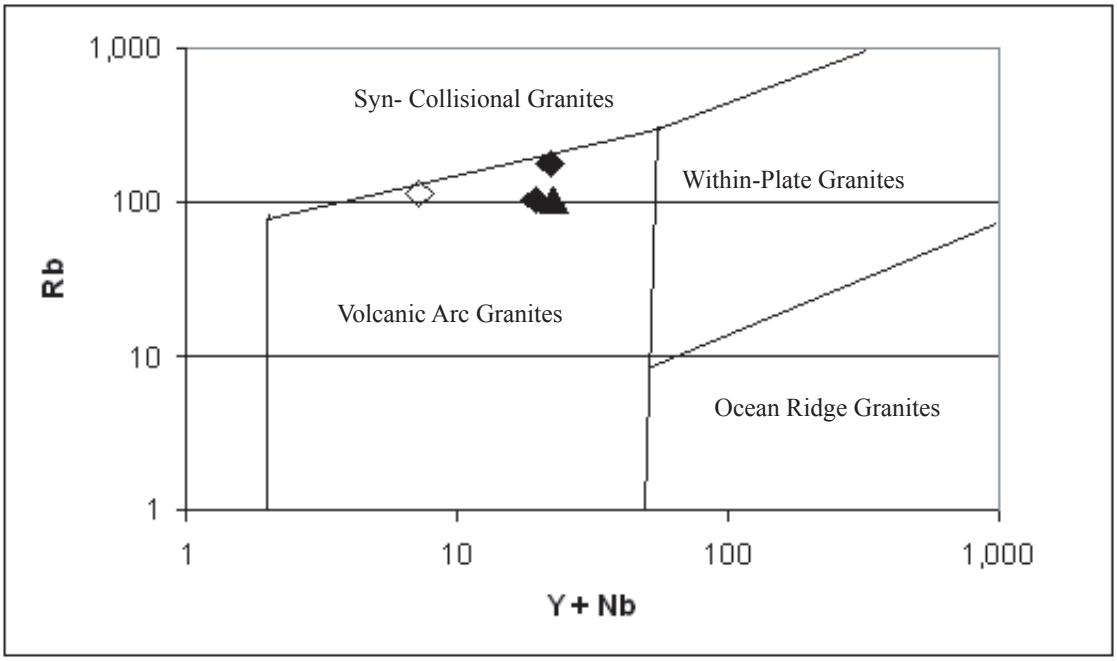

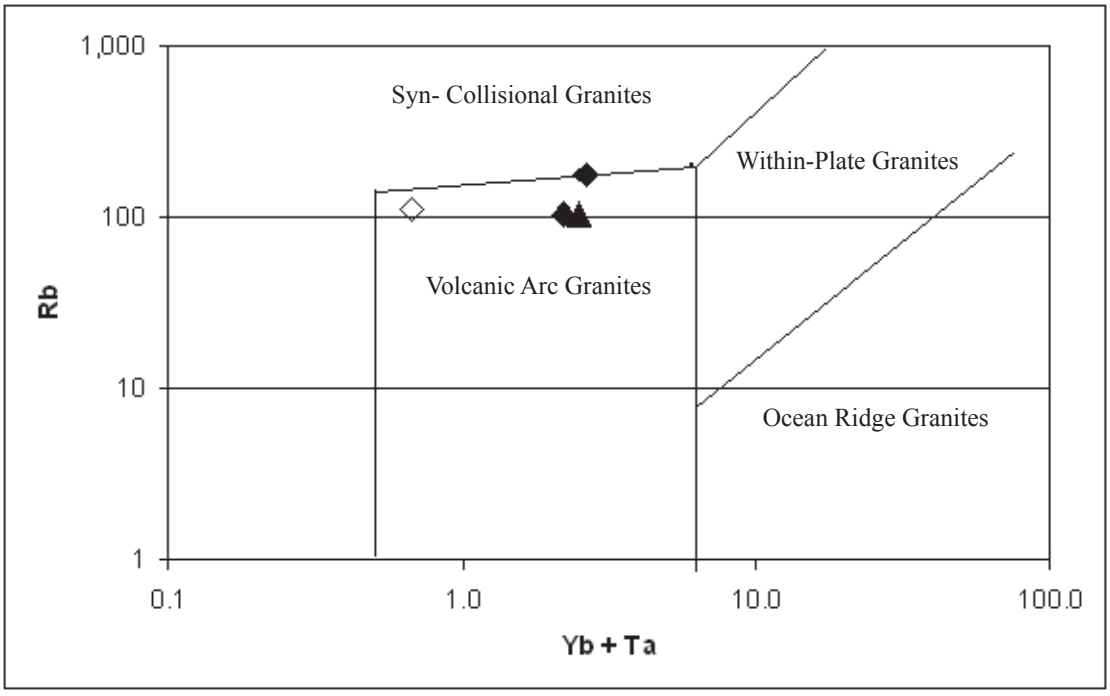

Figure 18, continued.

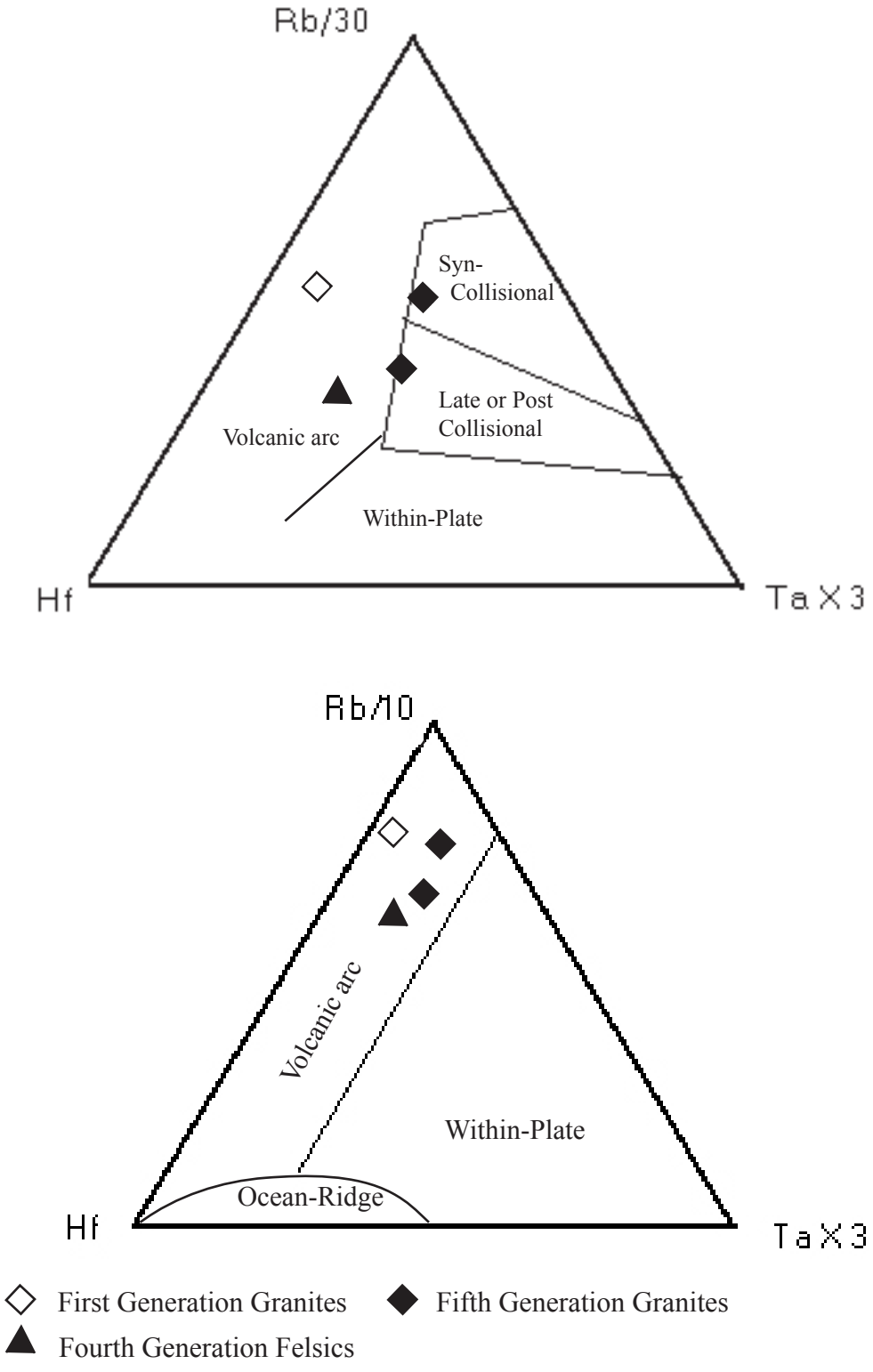

Figure 19. Felsics plotted Harris et al.'s (1986) diagrams for granitic rocks.

Standard AFM and other major element discrimination diagrams are inappropriate as the pervasive alteration is likely to have mobilized sodium and potassium (Rollinson, 1993). The application of some of the standard discrimination diagrams for basalts is questionable as some samples are significantly more silica enriched than the rocks to which the diagrams were calibrated (Table 3). On the other hand, Titanium, Manganese, and Phosphorous are generally assumed to be insensitive to hydrothermal processes (Rollinson, 1993) and are therefore used by Mullen (1983) as the basis for a discrimination diagram (Figure 20(a)). Samples converge on a triple point with samples 1 and 7 plotting as ocean-island alkali basalts, samples 32 and 33 as island-arc tholeiites, and the others as island-arc calc-alkaline basalts.

On Cabanis and Lecolle's (1989) Y-La-Nb diagram, data clusters across the calc-alkali volcanic arc basalt / continental basalt line, with samples 1, 5, and 3a plotting as continental basalts and the others as calc-alkali basalts (Figure 20(b)). On Wood's (1980) Hf-Th-Ta diagram, all data plot within the field for calc-alkaline volcanic arc basalts (Figure 20(c)).

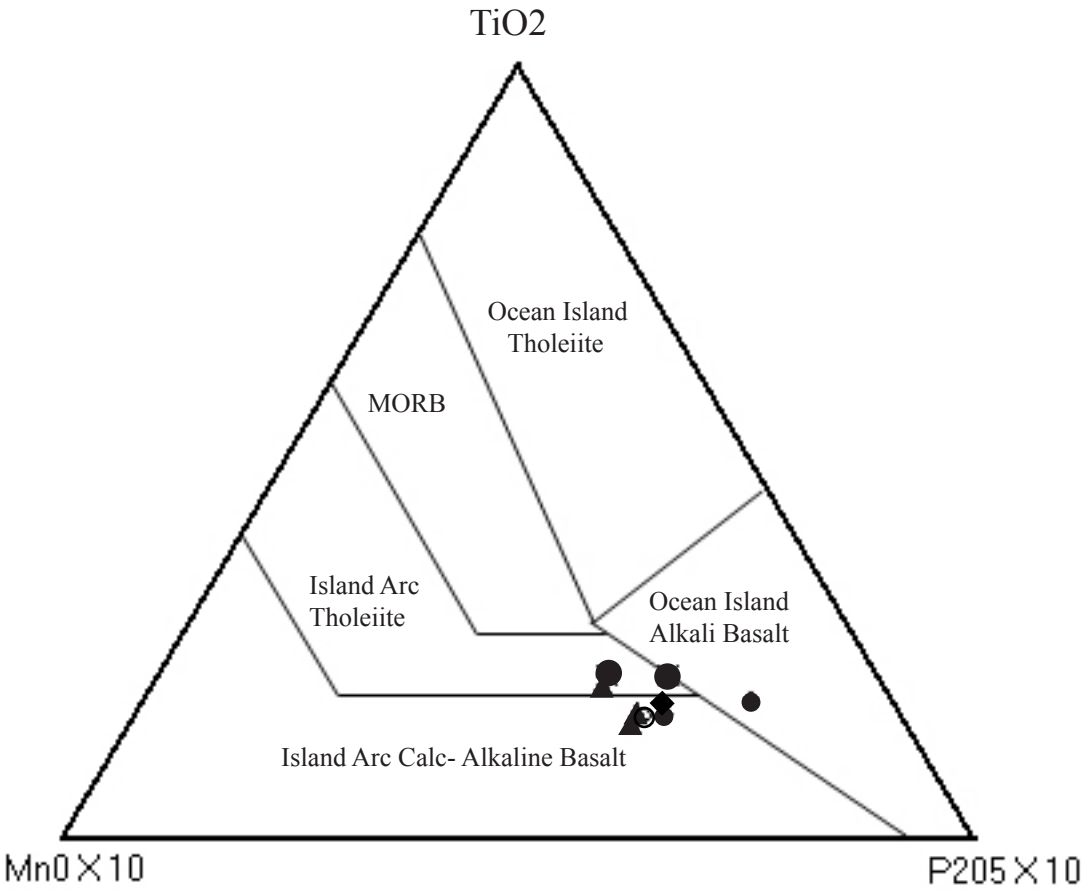

Figure 20. Discrimination diagrams for mafic rocks. (a): Mafics plotted on a Mn-Ti-P discrimination diagram proposed by Mullen (1983).

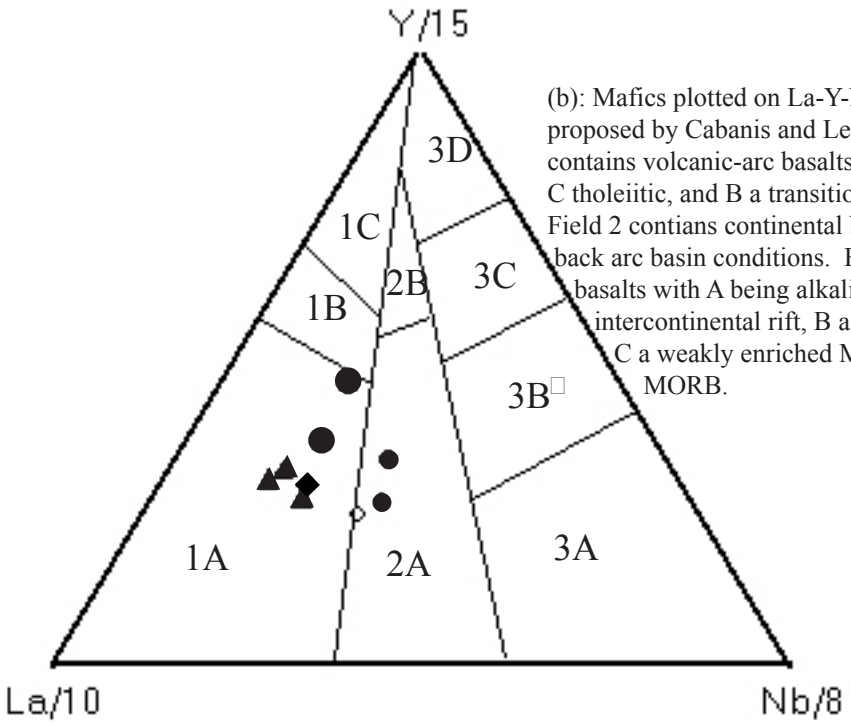

(b): Mafics plotted on La-Y-Nb discrimination diagram proposed by Cabanis and Lecolle (1989). Field 1 contains volcanic-arc basalts with A being calc-alkaline, C tholeiitic, and B a transition zone between A and C. Field 2 contians continental basalts, with B indicating back arc basin conditions. Field 3 contains oceanic basalts with A being alkali basalts from an intercontinental rift, B a strongly enriched MORB, C a weakly enriched MORB, and D a normal type MORB.

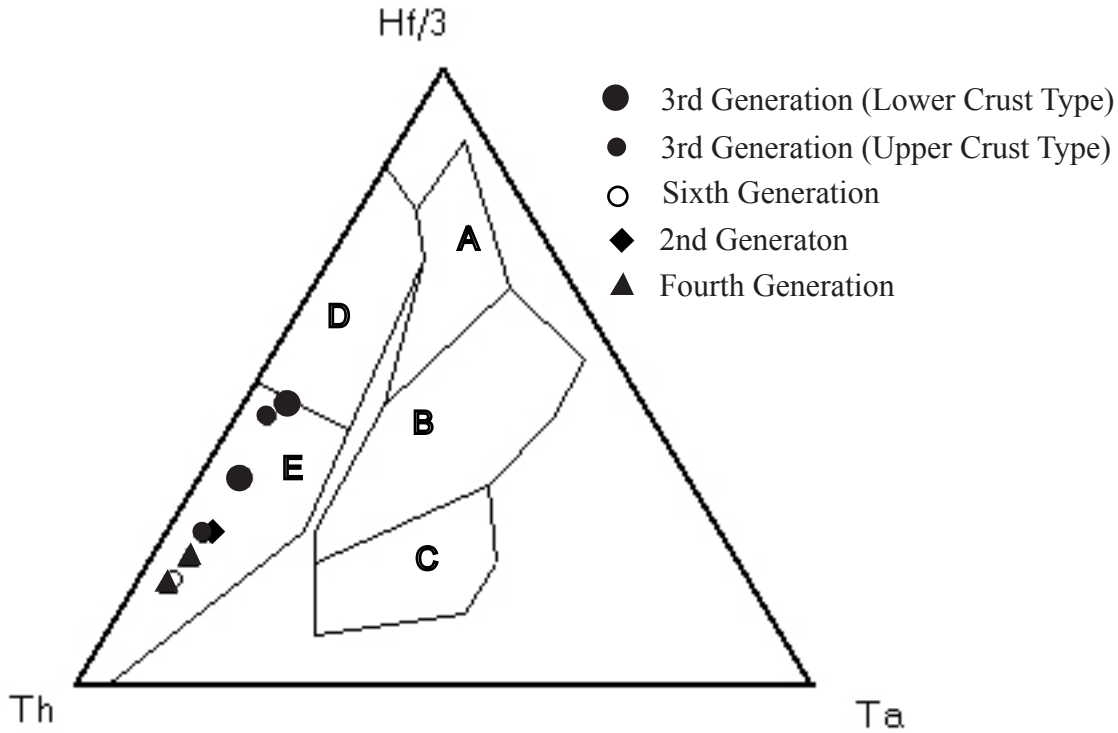

(c): Mafics plotted on Th-Hf-Ta discrimination diagram proposed by Wood (1980). The fields are A, normal type MORB; B, enriched type MORB; C, alkaline within-plate basalts; D, island-arc tholeiites; E, island-arc calc-alkaline basalts.

Figure 20 - continued.

Discussion

The alteration minerals present in some dikes are associated with subgreenschist facies metamorphism at 150°-300° C and 2-4 Kbars of pressure (Bucher and Frey, 2002). However, the pattern of alteration of mafic minerals (Figure 8) does not appear to have occurred as a single regional event, because alteration is not uniform and does not vary according to geography. In certain locations, such as the fourth generation dike swarms, percent alteration varies from 100% to near 0% within 20 m. I propose that the pattern of alteration is due to a heterogeneous distribution of heated fluids, possibly due to the intrusion of subsequent dikes or, in some cases, the latent heat and fluids of the dike event itself. This hypothesis explains the alteration patterns found in the fourth generation dike swarms. The heterogeneity of these dike swarms suggests that the dikes did not intrude simultaneously. Older dikes would be subject to the altering heat and fluids associated with younger dikes. In the western swarm, less altered dikes tend to be more felsic. If alteration corresponds to age, as I have suggested, then younger dikes within this swarm are progressively silica enriched. The south central area of alteration appears to center around the sixth generation mafic dikes (Figure 8). These dikes are themselves heavily altered and, being thick, may have had sufficient latent heat and fluids to alter many surrounding dikes. The eastern area displays near 100% alteration in all observed dikes. However, the dikes of this region are notably thick and may have likewise carried substantial latent heat and fluids.

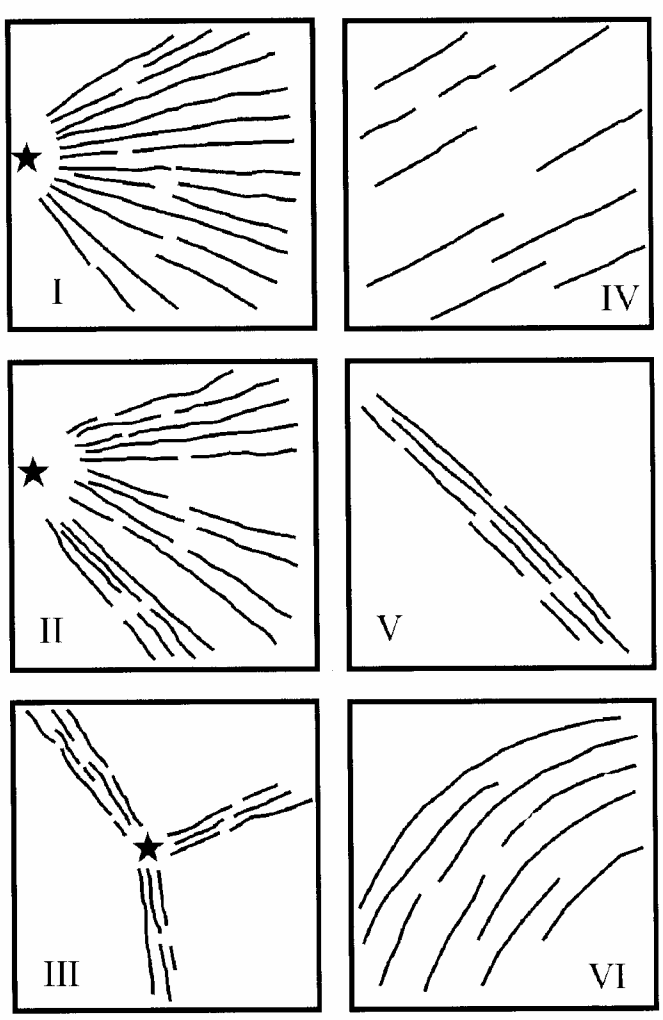

Figure 21. Ernst and Buchan's (2001) schematic for characteristic geometries of dike swarms. I – continuous fanning pattern. II – fanning pattern divided into sub swarms. III – sub swarms of sub parallel dikes that radiate from a common source. IV – sub parallel over a broad area. V- sub parallel over a narrow zone. VI – arcuate pattern. Stars locate magma source.

Ernst and Buchan (2001) propose six characteristic geometries of giant dike swarms observed on Earth, Venus, and Mars. These include three kinds of fanning geometries, sub parallel dikes over a broad area, sub parallel dikes over a narrow zone, and arcuate patterns (Figure 21). At least four of these six characteristic geometries are found within the study area. Generation six displays a continuous fan; generations one, two, and most of generation five are sub parallel over a broad area; generation four is sub parallel over a narrow zone; and generation three and the northwestern dikes of

generation five may display arcuate patterns (Figure 2). The unstudied apparent dikes north of the field area also have an arcuate pattern (Figure 7c). Fanning geometries are associated with domal uplift, usually associated with some sort of magmatic point source, such as a mantel plume; sub parallel geometries indicate that dikes have aligned according to regional tectonic stresses; and arcuate patterns are associated with transitions between fanning and sub parallel geometries or are part of a circumferential swarm (Ernst and Buchan, 2001). Circumferential swarms are abundant on Mars, but none have been positively identified on earth in association with mantle plumes (Ernst et al., 2001). If the third generation and the northwestern fifth generation are parts of circumferential swarms, then the remainder of the swarms must either be under sedimentary cover, lost to erosion, or removed by faults. It is perhaps conceivable that the abrupt transition between the south central area and the eastern area is a fault, though this was not indicated in the field. Additionally, the third generation dikes of the north central area do not particularly match with the arcuate pattern of third generation dikes of the south central area and would have to be ascribed to a different magmatic event and their petrographic similarities declared co-incidental. Faults need not be invoked to explain the northwestern area as circumferential. The classification of either of these two areas as transitions from fanning geometries to sub-parallel geometries is equally speculative, because we do not see either fanning geometries or non-arcuate sub-parallel geometries as end members of the transition. The northwest area would be particularly unusual as a transition between domal uplift and regional tectonic stress, as the outside curve or the arc is greater than 90 degrees. If transitional arcuate patterns can indeed

curve that acutely, some mechanism would need to be invented to explain why these dikes did not curve in a more energy efficient direction.

I propose that in the case of the south central area the regional tectonic stresses that controlled dike emplacement may have themselves been arcuate. While the sixth generation dikes intrude in a fanning pattern consistent with domal uplift, the base orientation is arcuate (Figure 6B). This implies that within the upper portions of the intrusion, domal uplift dominates as the control for dike orientation, but towards the base, stresses generating an arcuate pattern dominate (Figure 5).

Samples from the felsic generations plot in the same general region of the Zr/Hf v. Nb/Ta diagram (Figure 10). The first and fifth generations are easily distinguished on a chondrite normalized plot of the rare earth elements. Sample 17 was mapped as a first generation dike in the field, but its geochemical similarity to fifth generation sample 10 and its dissimilarity to first generation sample 30A suggest that it may have been initially miscategorized (Figure 13). The dike from which sample 17 is taken is cut by sixth generation dikes but not by third generation dikes, despite the abundance of such dikes in the vicinity. The structural orientation of the first generation (Figure 3) suggests a direction of least horizontal compressive stress oriented approximately N20°W. The magmatic source for this generation was highly fractionated and relatively small.

Unfortunately samples from the western and northwestern areas were not subject to geochemical analysis, so we have no geochemical link between the areas with fifth generation dikes. The western dikes show two groups, one trending around N60°E and the other at N50°W (Figure 3). If these groups represent a single stress field applied to a single event, the least horizontal compressive stress is oriented N5°E. This composite

stress is moderately similar to the N15°E pole to the strike directions of the eastern dikes (Figure 3). This general similarity in stress fields suggests that the two sets of dikes might be part of the same event. Either way, significant quantities of felsic material were injected into such stress fields toward the end of the series of the dike events in this terrane.

The uniqueness of the rare earth element distribution present in sample 25B (Figure 14), the one sample from the western dike swarm, suggests that the western dike swarm may have been sourced differently from the eastern dike swarm. The base orientations of the dike swarms are nearly identical, N54°W and N57°W respectively. Base extensional stress for the fourth generation is therefore approximately N25°E. The stresses at the present surface differ somewhat more largely between the two swarms, indicating different surface stresses during dike emplacement (Figure 5).

With the exception of samples 7 and 32, the REE distributions of second, third, and sixth generations, and the fourth generation eastern dike swarm resemble each other (Figure 12). When normalized to MORB values, trace element data for samples 7 and 32 resemble values for the lower crust (Figure 17). Sample 7 is the most southerly of the analyzed third generation samples and sample 32 is the most northerly. Thus, it seems unlikely that the difference in REE and trace element distributions in the third generation results from two unique events. The fact that these dikes are more primitive, resembling values for the lower crust, may indicate that many third generation dikes were subject to upper crustal contamination. More analyses are required to determine the distribution of this contamination. The arcuate stresses of the south central area aside, the third generation has its largest peaks at N40°E and N30°W (Figure 3). If these are parts of the

same event, the least horizontal compressive stress trends N85°E, exactly orthogonal to the least horizontal compressive stress in the fifth generation.

These changes in stress orientation suggest a convoluted history of stress fields, where least horizontal compressive stress was initially approximately NNW-SSE during the emplacement of the first generation. The second generation is too complex and poorly studied for a determinative statement about the orientation of its stress fields. By the emplacement of third generation, stress was oriented approximately E-W. By the fourth generation stress was oriented approximately NNE-SSW. And by the fifth generation it was almost N-S.

The mid Permian closure of the Solonker Ocean and the subsequent collision of the North China block with the Mongolian terranes occurred when the Monglian terranes were aligned nearly East-West (Sengör and Natal'in, 1996). It is therefore conceivable that the collisional forces from the North China Block were oriented N5°E and the complementary least horizontal compressive stress oriented N85°E. If this hypothesis is true, a precise date of third generation dikes would provide some additional age control for this collision, which is presently based on transitions in sedimentary sequences (Yue et al., 2001). The subsequent changes in dike orientation may relate to the subsequent rotation of the North China block toward the Siberian Craton (Sengör and Natal'in, 1996), though geochronological results are needed to test these hypotheses.

The general agreement of the various tectonic discrimination diagrams employed is that the dikes formed in a volcanic arc environment (Figures 18-20). It is possible that some within-plate processes, collisional environments, and continental material affected the chemistry of some dikes. But a volcanic arc setting is most consistent with the data

and most consistent with the general history of the Mongolian accreted terranes (Sengör and Natal'in, 1996).

Conclusions

Petrographic data, structural data, and cross cutting relationships suggest at least six dike events within the granodiorites of the Khövsgöl-Ulaanbadrakhin Terrane. Geochemical data suggests that at least five types of magma sources or fractionation were part of these dike events. These magma types do not correspond exactly to the structural and petrographic generations; certain types extend across generations and certain generations contain multiple types. However, the small number of geochemical samples prevents strong geochemical conclusions. The diverse orientations of the various generations indicate a tectonic history in which the direction of the least principal horizontal compressive stress rotated 335° during the series of dike emplacement events.

Acknowledgements

I would like to acknowledge several people for their contributions to this project. In the field E. Molor worked as my partner. We subsequently have corresponded and discussed several aspects of the project and are co-authors on a Keck abstract. Some of the field driving and navigation was done by D. Sengee. Chris Carson helped with field navigation and offered advice in the field. Kevin Pogue gave field advice and has subsequently advised me on drafts of my Keck abstract. The entire Keck expedition was only made possible through the organizational efforts of Bob Carson and T. Bayasgalan.

Cari Johnson provided aerial photographs that proved invaluable in the field, and has since provided access to digital topographic maps and aerial photographs, suggested references, and provided professional contacts. Cam Davidson has served as my Carleton advisor, edited drafts, and given several helpful suggestions of how to proceed. Ben Harrison has advised me on how best to analyze my geochemical data and has given technical assistance in the preparation of samples for and the operation of the XRF machine. Paul Renne has offered to do geochronological work on some samples. Sebastien Nomade gave technical assistance in the separation of hornblende and zircon grains for geochronological analysis. Numerous geology seniors have advised me on the operation of computer software.

Cited References

Anderson, E. M., 1963, The dynamics of faulting and dyke formation with applications to Britain: Edinburgh, Oliver and Boyd, 206 p.

Bayasgalan, T., 2003, Personal Communication.

Baynaa, 2003, Unpublished maps.

Boynton, W. V., 1984, Cosmochemistry of the rare earth elements; meteorite studies.

Bucher, K., and Frey, M., 2002, Petrogenesis of metamorphic rocks: Berlin, Springer, xv, 341 p.

Cabanis, B., and Lecolle, M., 1989, Le diagramme La/10-Y/15-Nb/8; un outil pour la discrimination des series volcaniques et la mise en evidence des processus de melange et/ou de contamination crustale.: Comptes Rendus de l'Academie des Sciences, Serie 2, Mecanique, Physique, Chimie, Sciences de l'Univers, Sciences de la Terre, v. 309, no. 20, p. 2023-2029.

Campbell, I. H., 2001, Identification of ancient mantle plumes: Special Paper - Geological Society of America, v. 352, p. 5-21.

Ernst, R. E., and Buchan, K. L., 2001, The use of mafic dike swarms in identifying and locating mantle plumes: Special Paper - Geological Society of America, v. 352, p. 247-265.

Ernst, R. E., Grosfils, E. B., and Mege, D., 2001, Giant dike swarms; Earth, Venus, and Mars: Annual Review of Earth and Planetary Sciences, v. 29, p. 489-534.

Graham, S. A., Hendrix, M. S., Johnson, C. L., Badamgarav, D., Badarch, G., Amory, J., Porter, M., Barsbold, R., Webb, L. E., and Hacker, B. R., 2001, Sedimentary record and tectonic implications of Mesozoic rifting in Southeast Mongolia: Geological Society of America Bulletin, v. 113, no. 12, p. 1560-1579.

Harris, N. B. W., Pearce, J. A., and Tindle, A. G., 1986, Geochemical characteristics of collision-zone magmatism: Geological Society Special Publications, v. 19, p. 67-81.

Hendrix, M. S., Beck, M. A., Badarch, G., and Graham, S. A., 2001, Triassic synorogenic sedimentation in southern Mongolia; early effects of intracontinental deformation: Memoir - Geological Society of America, v. 194, p. 389-412.

Heubeck, C., 2001, Assembly of Central Asia during the middle and late Paleozoic: Memoir - Geological Society of America, v. 194, p. 1-22.

Johnson, C. L., Webb, L. E., Graham, S. A., Hendrix, M. S., and Badarch, G., 2001, Sedimentary and structural records of late Mesozoic high-strain extension and strain partitioning, East Gobi Basin, southern Mongolia: Memoir - Geological Society of America, v. 194, p. 413-433.

Kast, P., and Manchuk, N., 2004, New Evidence for Quaternary Faulting in Southeast Mongolia.

Lamb, M. A., and Badarch, G., 2001, Paleozoic sedimentary basins and volcanic arc systems of southern Mongolia; new geochemical and petrographic constraints: Memoir - Geological Society of America, v. 194, p. 117-149.

Lamb, M. A., Hanson, A. D., Graham, S. A., Badarch, G., and Webb, L. E., 1999, Left-lateral sense offset of upper Proterozoic to Paleozoic features across the Gobi Onon, Tost, and Zuunbayan faults in southern Mongolia and implications for

other Central Asian faults: Earth and Planetary Science Letters, v. 173, no. 3, p. 183-194.

Mullen, E. D., 1983, $MnO/TiO_2/P_2O_5$; a minor element discriminant for basaltic rocks of oceanic environments and its implications for petrogenesis: Earth and Planetary Science Letters, v. 62, no. 1, p. 53-62.

Pearce, J. A., Harris, N. B. W., and Tindle, A. G., 1984, Trace element discrimination diagrams for the tectonic interpretation of granitic rocks: Journal of Petrology, v. 25, no. 4, p. 956-983.

Rollinson, H. R., 1993, Using geochemical data : evaluation, presentation, interpretation: Harlow, Essex, England, Longman Scientific & Technical, xxvi, 352 p.

Sengör, A. M. C., and Natal'in, B. A., 1996, Paleotectonics of Asia: fragments of a synthesis, *in* Yin, A., and Harrison, T. M., eds., The Tectonic Evolution of Asia: World and Regional Geology Series, p. 486-640.

Sun, S. S., and McDonough, W. F., 1989, Chemical and isotopic systematics of oceanic basalts; implications for mantle composition and processes: Geological Society Special Publications, v. 42, p. 313-345.

Taylor, S. R., and McLennan, S. M., 1981, The composition and evolution of the continental crust; rare earth element evidence from sedimentary rocks: Philosophical Transactions of the Royal Society of London, Series A: Mathematical and Physical Sciences, v. 301, no. 1461, p. 381-399.

Weaver, B. L., and Tarney, J., 1984, Empirical approach to estimting the composition of the continental crust: Nature, v. 310, no. 5978, p. 575-577.

Website, 2003, University of Marland Global Land Cover Facility, University of Maryland.

Winchester, J. A., and Floyd, P. A., 1977, Geochemical discrimination of different magma series and their differentiation products using immobile elements: Chemical Geology, v. 20, no. 4, p. 325-343.

Wood, D. A., 1980, The application of a Th-Hf-Ta diagram to problems of tectonomagmatic classification and to establishing the nature of crustal contamination of basaltic lavas of the British Tertiary volcanic province: Earth and Planetary Science Letters, v. 50, no. 1, p. 11-30.

Yue, Y., Liou, J.-G., and Graham, S. A., 2001, Tectonic correlation of Beishan and Inner Mongolia orogens and its implications for the palinspastic reconstruction of North China: Memoir - Geological Society of America, v. 194, p. 101-116.

Zorin, Y. A., Belichenko, V. G., Turutanov, E. K., Kozhevnikov, V. M., Ruzhentsev, S. V., Dergunov, A. B., Filippova, I. B., Tomurtogoo, O., Arvisbaatar, N., Bayasgalan, T., Biambaa, C., and Khosbayar, P., 1993, The South Siberia-central Mongolia transect: Tectonophysics, v. 225, no. 4, p. 361-378.